Solid State Solvation: a fresh view

Brunella Bardi, Davide Giavazzi, Elena Ferrari, Alessandro Iagatti, Mariangela Di Donato, D. K. Andrea Phan Huu, Francesco Di Maiolo, Cristina Sissa, Matteo Masino, Andrea Lapini and Anna Painelli

July 19, 2023

Citation numbers refer to the specific bibliography of this document

Contents

1 Experimental procedures and additional data

1.1 Fluorescence spectra and the self-absorption problem

A delicate issue posed by fluorescence spectroscopy concerns the choice of the sample concentration, which must be low enough to minimize trivial inner filter effects. Fig.S1 compares the emission spectra of DCM and NR dispersed in mCBPCN films, obtained either by spin coating or drop casting, and with loading varying from 1% to 0.01% by weight. Upon increasing the dye loading

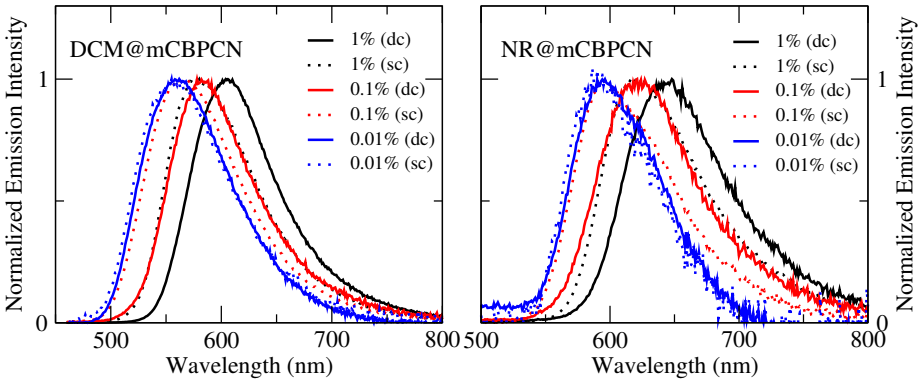

Figure S1: Emission spectra of DCM and NR in mCBPCN films prepared by drop-casting (dc) or spin-coating (sc) at different concentrations (expressed in %wt). Emission spectra were obtained subtracting the emission spectrum of the pure host.

a red-shift of the emission band is clearly seen, more pronounced in drop cast films than in spin-coated samples. This behavior is safely ascribed to a parasitic self-absorption (or inner-filter) phenomenon, i.e., to the re-absorption of the light emitted by the dye, as due to the sizable absorbance of the samples in the region where emission and absorption bands do overlap. The red-shift increases with the absorbance, i.e. with dye concentration and the sample thickness. Indeed self-absorption affects more drop-cast than spin coated films, since typically upon drop-casting, thicker films are obtained than upon spin coating.

Fig. S1 shows that at low enough concentrations, emission spectra of thin samples are virtually unaffected by further dilution, indicating the ideal condi-

tions for fluorescence measurements. In this work, low dye loading is required for drop-cast films (down to 0.01%), while spin-coating allows to work with slightly larger concentrations, up to 0.1%. Because drop-cast films of some hosts (mCP and DPEPO) are prone to crystallization, in our fluorescence study we focused on 0.1% spin-coated films, which offer a good compromise between signal intensity and minimization of self-absorption.

We underline that the detrimental effect of self-absorption on fluorescence, being proportional to the sample absorbance, is especially tricky for probes characterized by high molar extinction coefficients, like DCM and Nile Red ($> 4 \times 10^4$ M^{-1} cm^{-1}). For typical TADF dyes, with poorly conjugated donor and acceptor moieties, the CT bands are much weaker, leading to less stringent requirements on fluorescence measurements.

1.2 Raman spectra

Unlike fluorescence, Raman scattering do not suffer from inner-filter effects, allowing for the characterization of highly absorbing samples, e.g., concentrated samples (> 0.1% in this work) or thick films (as obtained by drop-casting). Indeed, high concentrations and/or thickness must be used to achieve good signal-to-noise ratios. For this reason, the results of Raman spectra were collected from drop-cast films with 1% dye loading.

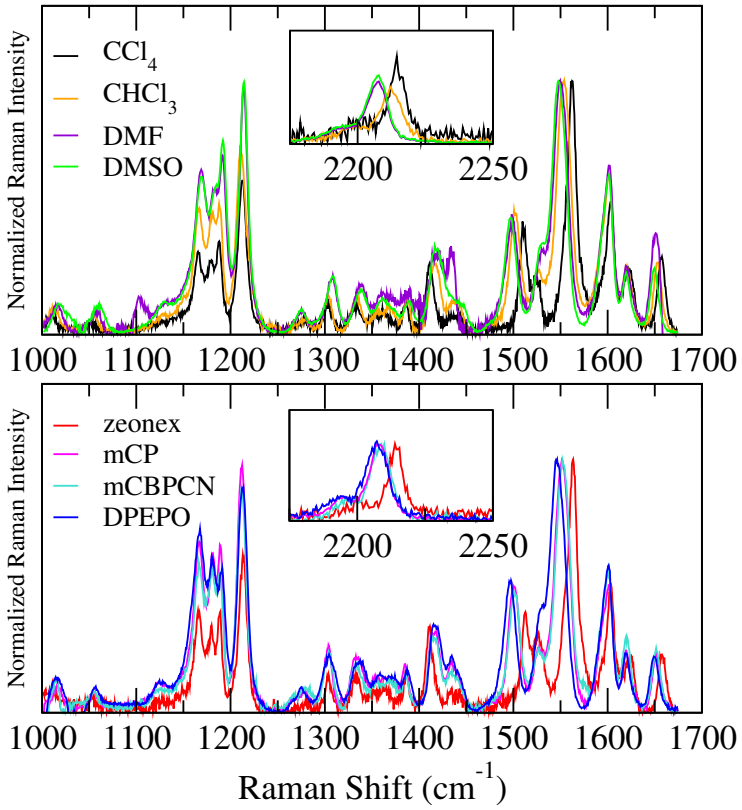

Figure S2: Raman spectra of DCM in different solvents (top panel) and matrices (bottom panel).

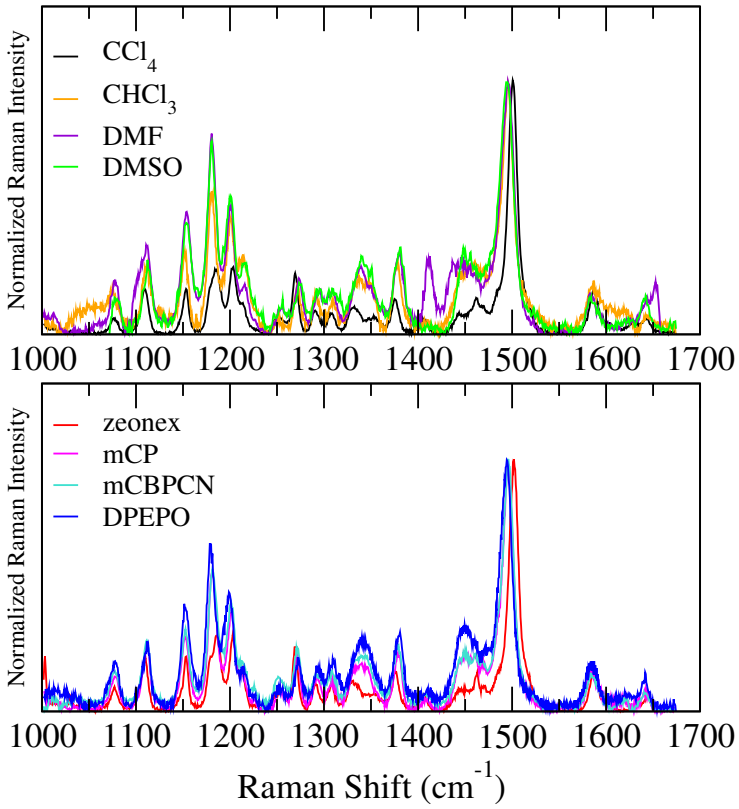

Figure S3: Raman spectra of Nile Red in different solvents (top panel) and matrices (bottom panel).

1.3 Time resolved emission spectra (TRES), TCSPC technique

TRES were collected on the same samples used for fluorescence measurements. The time-evolution of TRES, recorded with the time-correlated single-photon counting (TCSPC) technique, was analyzed using a global analysis program package (glotaran: https://glotaran.org)[**JSSGlotaran**]. The adopted kinetic scheme was constituted by a three component unidirectional-sequential model with increasing lifetimes, and the evolution of each component is described by a single exponential decay. The three spectral components allowed us to reproduce the simultaneous frequency-shift of the fluorescence emission peak (due to the solvent relaxation) and the decay of the fluorescence spectrum (due to population relaxation). The entire temporal trace was fitted by the convolution of the the model function with a Gaussian-shaped instrumental response function whose full-width at half maximum is an adjustable fitting parameter. The procedure leads to a raw estimate of the time resolution (0.3 +/- 0.2 ns), and of the origin of the time axis.

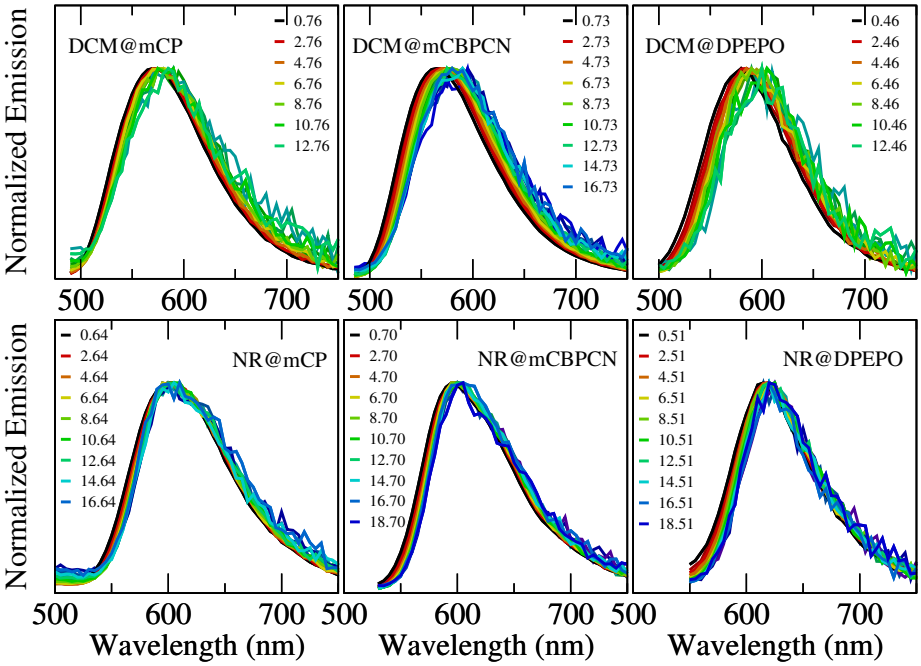

Figure S4: Time-resolved emission spectra (TRES) of DCM (top panels) and NR (bottom panels) in different matrices. Time units: ns.

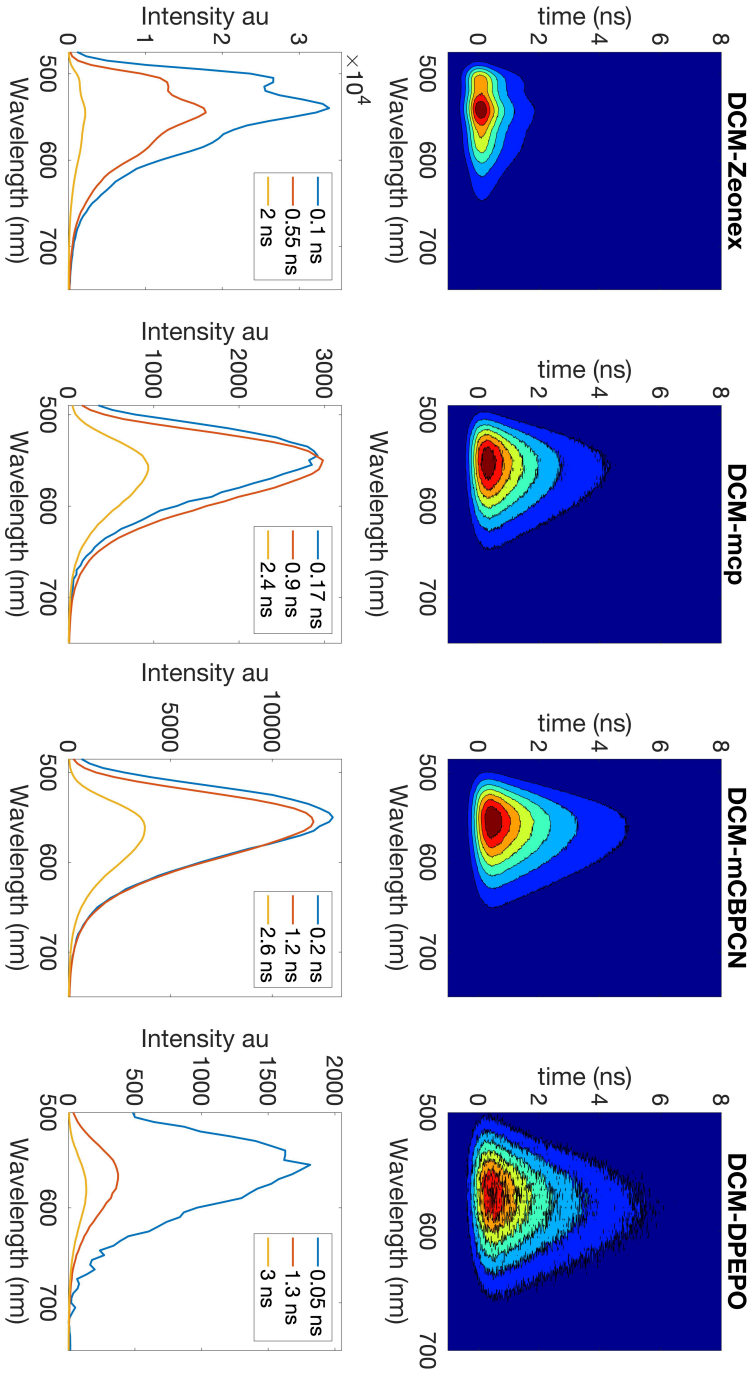

Figure S5: Experimental time-resolved emission spectra (TRES) of DCM (top panels) and spectral components (lower panel) used to simulate spectral evolution of TRES. Time constant for each spectral component are reported as an inset in lower panels. Time units: ns.

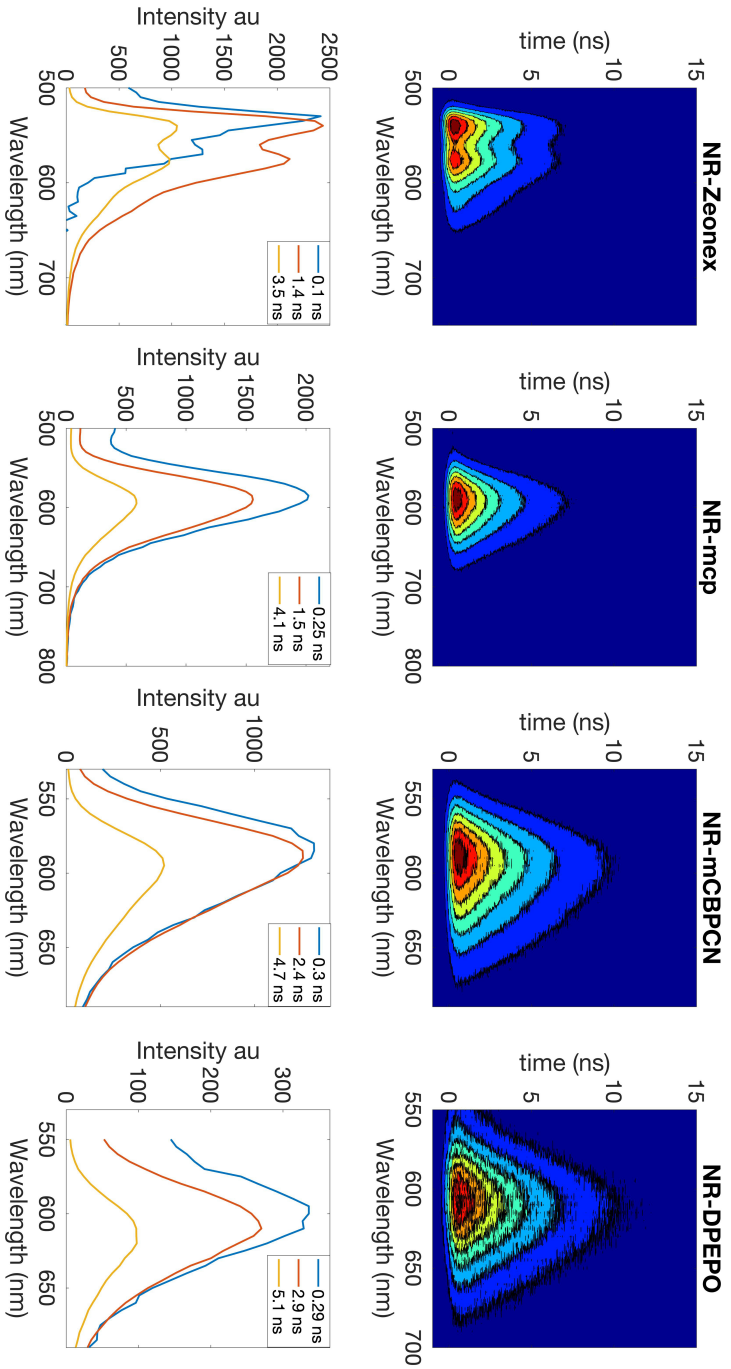

Figure S6: Experimental time-resolved emission spectra (TRES) of NR (top panels) and spectral components (lower panel) used to simulate spectral evolution of TRES. Time constant for each spectral component are reported as an inset in lower panels Time units: ns.

1.4 Pump-probe spectra

Self-absorption is not an issue for pump-probe spectra, so we collected data on drop-cast films at 1% loading, as to improve the signal to noise ratio.

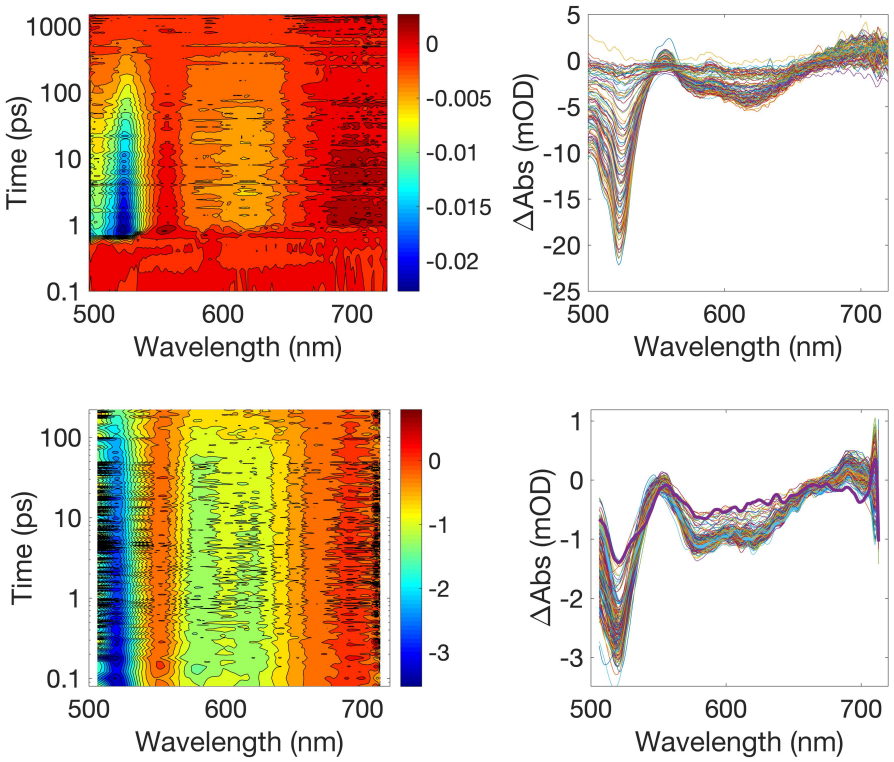

Figure S7: Pump-Probe spectra of NR in Zeonex, recorded with the LR-pp setup (upper panels) and with US-pp setup (lower panels).

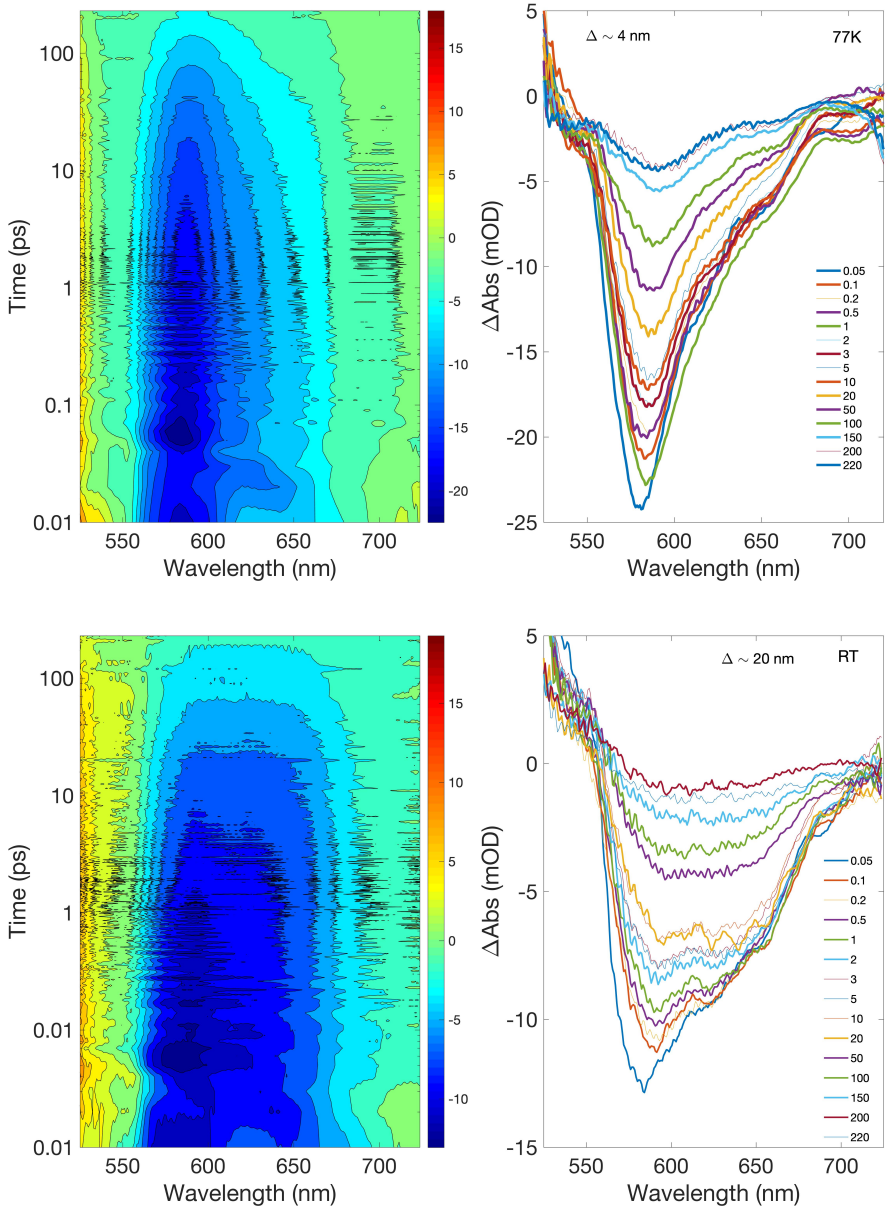

Figure S8: Pump probe spectra of NR in mCBPCN matrix (US-pp setup), at 77K (upper panels) and at room temperature (lower panels). The time-dependence of the maximum of the stimulated emission band at the two temperatures is reported in Fig. S10, top panel.

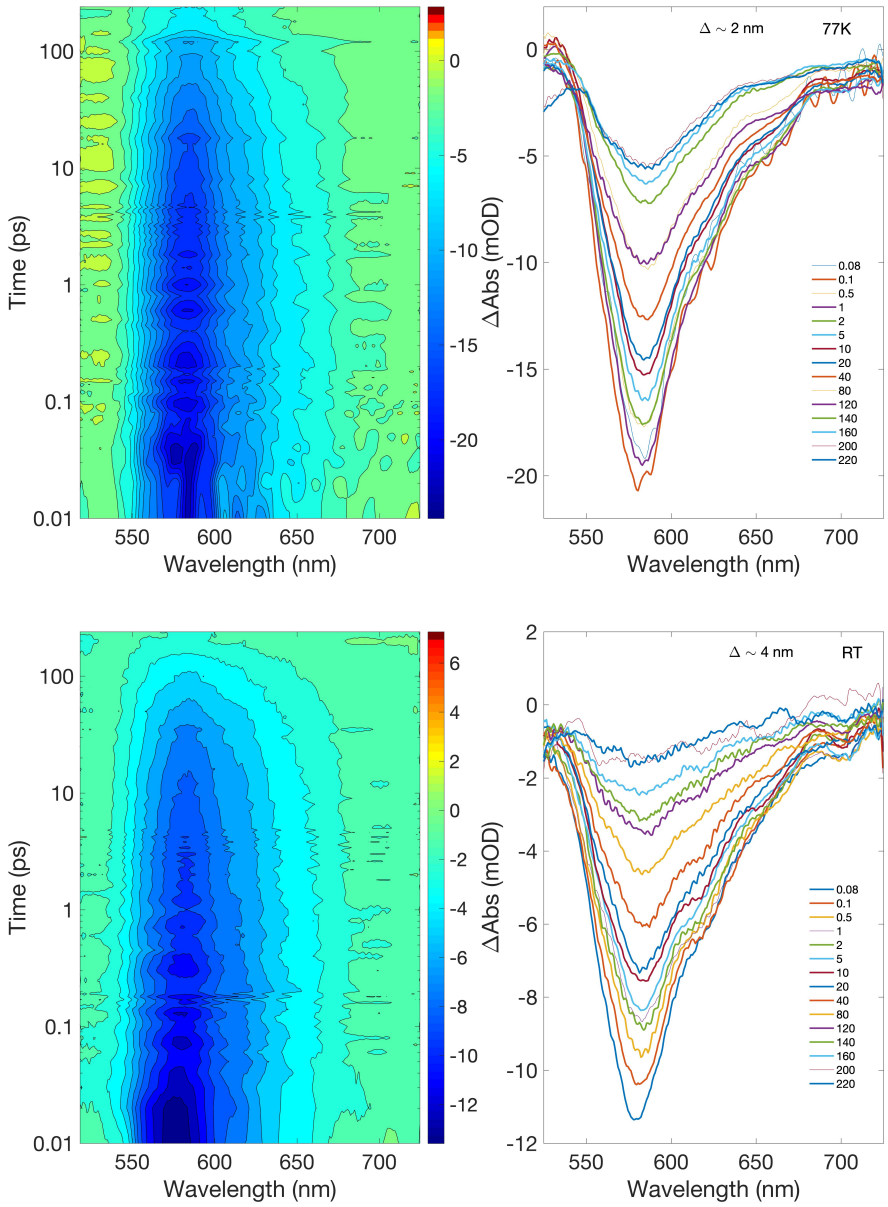

Figure S9: Pump probe spectra of NR in DPEPO matrix (US-pp setup), at 77K (upper panels) and at room temperature (lower panels). The time-dependence of the maximum of the stimulated emission band at the two temperatures is reported in Fig. S10, bottom panel.

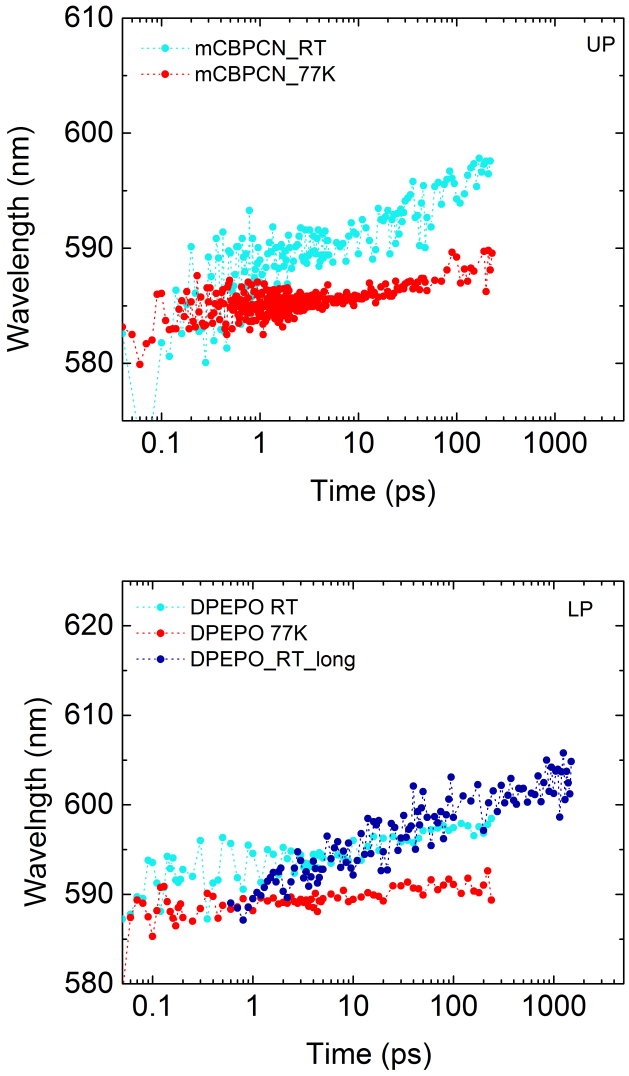

Figure S10: Comparison between the temporal evolution of the wavelength of the maximum of the stimulated emission at Room temperature (blue and light blue dots) and at 77K (red dots), for NR in mCBPCN matrix (upper panel) and DPEPO (lower panel).

2 The model: dyes in liquid solvents

2.1 Steady-state spectra

The low-energy photophysics of NR and DCM in solution is well described in terms of essential state models, a family of parametric Hamiltonians developed and extensively validated in the last two decades. Specifically, our dyes are π-conjugated molecules with an electron donor and an electron-acceptor group, D-π-A. Their low-energy physics is described in terms of two electronic states, $|N\rangle$ and $|Z\rangle$, corresponding to the neutral $D-\pi-A$ and zwitterionic $D^+-\pi-A^-$ structures, respectively. A single harmonic vibrational coordinate, $\hat{Q} = (\hat{d}^\dagger + \hat{d})/\sqrt{2}$, accounts for the variation of the molecular structure when the electron is transferred from the D to the A site. The Hamiltonian reads:

$$\hat{H}_{mol} = -\tau\hat{\sigma}_x + \left[2z_0 - \sqrt{\hbar\omega_v\varepsilon_v}\left(\hat{d}^\dagger + \hat{d}\right)\right]\hat{\rho} + \hbar\omega_v\left(\hat{d}^\dagger\hat{d} + \frac{1}{2}\right) \qquad (1)$$

where $\hat{\sigma}_x = |N\rangle\langle Z| + |Z\rangle\langle N|$ and $\hat{\rho} = |Z\rangle\langle Z|$ are the hopping and the ionicity operators. The molecular model is fully defined by four parameters: z_0, half the energy gap between the two electronic states, τ the mixing matrix element, ω_v the frequency of the vibrational mode and ϵ_v the vibrational relaxation energy. The dipole moment operator is defined as $\hat{\mu} = \mu_0\hat{\rho}$, thus neglecting all matrix elements of $\hat{\mu}$ except for μ_0, the large dipole associated with the $|Z\rangle$ state. While μ_0 would introduce an additional parameter, it is irrelevant for our calculations, where absolute absorption intensities are not addressed.

To address polar solvation, we rely on the Onsager model that describes the solute-solvent interaction in the dipolar approximation. Specifically, a polar medium surrounding a solute molecule generates at the solute location an electric field, the reaction field, proportional to the molecular dipole moment. It is convenient to define the effective solvation field F in energy units so that the Hamiltonian of the molecule in solution reads:

$$\hat{H} = \hat{H}_{mol} - F\hat{\rho} + \frac{F^2}{4\epsilon_{or}} \qquad (2)$$

where the second term describes the interaction between the field (or, to be specific, the field component parallel to the molecular dipole moment) and the

solute molecule, and the last term accounts for the elastic restoring force with ϵ_{or} measuring the solvent relaxation energy. Polar solvation is related to the slow, typically overdamped, motion of polar solvent molecules around the solute. Accordingly, its kinetic energy is neglected and F is treated as a classical coordinate.

For each value of F, the Hamiltonian in eq. 2 is written on the basis obtained as the direct product of the two electronic states $|N\rangle$ and $|Z\rangle$ and the the first M eigenstates of the harmonic oscillator associated with the vibrational coordinate, setting M to a large enough value to reach convergence (M=15 in this work). The diagonalization of the matrix Hamiltonian gives the numerically exact non-adiabatic vibronic eigenstates of the molecule. These $F-$dependent eigenstates are used to calculate F-dependent absorption A, fluorescence F and Raman R spectra using the following expressions:

$$A(\omega;F) \propto \omega \sum_{i>1} |\mu_{i1}(F)|^2 \exp\left(-\frac{(\omega_{i1}(F)-\omega)^2}{2\sigma^2}\right) \tag{3}$$

$$F(\omega,F) \propto (\omega)^3 \sum_{i<f} |\mu_{if}(F)|^2 \exp\left(-\frac{(\omega_{if}(F)-\omega)^2}{2\sigma^2}\right) \tag{4}$$

$$R(\omega,F) \propto \mathrm{Im}\left\{\sum_{i>1} \frac{1}{\omega_{i1}(F)-\omega-i\gamma}\left(\sum_{j>1}\frac{2\mu_{1j}(F)\mu_{ji}(F)}{\omega_{j1}(F)}\right)\right\} \tag{5}$$

where i,j run on the eigenstates (i=1 is the ground states) and the fluorescent state f (the Kasha state) is identified as the first eigenstate of the electronically excited manifold. $\omega_{ij}(F)$ and $\mu_{ij}(F)$ are the transition frequency and dipole moment of the $j \to i$ transition. A Gaussian lineshape with standard deviation σ is assigned to each transition for the absorption and fluorescence spectra, while a Lorentzian lineshape with half width at half maximum γ is used for Raman spectra. In this work $\sigma = 0.055$ eV, $\gamma = 0.0005$ eV.

Finally, the spectra of the solvated dye , in top panels of Fig. 8 (the main text) and of Fig. S11 are calculated averaging over the field distributions as relevant to the ground state, for the absorption and Raman spectra, and over the field distribution relevant to the Kasha state, for the steady-state fluorescence spectra. Of course this approach works well for fluorescence spectra in

liquid (non-viscous) solvents, where the relaxation time of the solvents, in the ps timewindow, ensure the full equilibration of the solvent around the excited solute before fluorescence takes place.

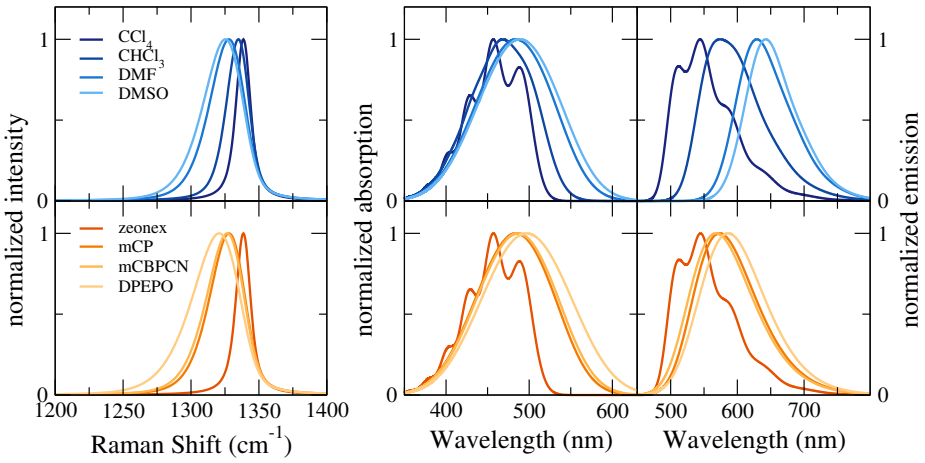

Figure S11: DCM: calculated steady state spectra (from left to right: Raman, absorption and fluorescence spectra). Top panels and bottom panels refer to liquid and solid samples, respectively. Molecular parameters are listed in Table 1, main text, the same solvent relaxation energies, ϵ_{or}=0.1, 0.32, 0.65, 0.75 eV for CCl_4, $CHCl_3$, DMF and DMSO, respectively, apply to both absorption and fluorescence spectra. For matrices, Raman and absorption spectra are simulated setting the solvent relaxation energy to ϵ_{or}=0.1, 0.65, 0.7, 0.9 eV for Zeonex, MCP, MCBPCN and DPEPO, respectively. For fluorescence spectra the relaxation energy of each matrix is partitioned into a static component set to ϵ_{or}^{st}=0.0, 0.45, 0.55, 0.7 eV for Zeonex, MCP, MCBPCN and DPEPO, respectively, and a dynamical component set, for the same matrices, to ϵ_{or}^{dyn}=0.1, 0.2, 0.15, 0.2 eV.

2.2 Time-resolved spectra

To address time-resolved spectra, we must account for the concurrent relaxation of the molecule and of the environment after the impulsive excitation of the dye. As for the dye relaxation, we adopt the Redfield approach and introduce a bath of harmonic oscillators $\sum_i \hbar\omega_i(\hat{b}_i^\dagger\hat{b}_i + 1/2)$ where $\hat{b}_i^{(\dagger)}$ is the boson annihilation

(creation) operator for the bath oscillator with frequency ω_i. Linear coupling between the solute coordinate $\hat{Q}$ and the bath coordinates is introduced:

$$\hat{H}_{SB} = \hat{Q} \sum_i g_i (\hat{b}_i^\dagger + \hat{b}_i)/\sqrt{2} \tag{6}$$

where g_i measures the strength of the coupling between $\hat{Q}$ and the i-th bath coordinate, usually defined in terms of the spectral density $\mathcal{I}(\omega) = \sum_i |g_i|^2 \delta(\omega - \omega_i)$. Here we consider a constant spectral density $\mathcal{I}(\omega) = \hbar^2 \gamma / \pi$, so that a single parameter fully describes the coupling between the system and the bath.

The solvent relaxation can be described by the Smoluchowski equation, that is coupled to the Redfield relaxation in the following quantum-classical master equation:

$$\begin{aligned}
\frac{\partial}{\partial t}\sigma_{ab}(F;t) = & -i\omega_{ab}\sigma_{ab}(F;t) + \sum_{cd} R_{ab,cd}\sigma_{cd}(F;t) \\
& - \frac{F}{i\hbar}\sum_c \left(\rho_{ac}\sigma_{cb}(F;t) - \sigma_{ac}(F;t)\rho_{cb}\right) \\
& - \frac{\varepsilon_{or}}{\tau_l}\sum_c \left(\rho_{ac}\frac{\partial \sigma_{cb}(F;t)}{\partial F} + \frac{\partial \sigma_{ac}(F;t)}{\partial F}\rho_{cb}\right) \\
& + \frac{1}{\tau_l}\frac{\partial}{\partial F}\left(F\sigma_{ab}(F;t) + k_B T 2\varepsilon_{or}\frac{\partial}{\partial F}\sigma_{ab}(F;t)\right)
\end{aligned} \tag{7}$$

where $\sigma_{ab}(F;t)$ is the F-dependent density matrix written on the basis of the eigenstates of the molecular Hamiltonian in Eq. 1. The first line in the above equation describes the Liouvillian dynamics, with ω_{ab} being the frequency of the $b \rightarrow a$ transition, and the Redfield relaxation. The second and third lines describe the effect of the solvent on the solute and *vice versa*, and the last line accounts for the Smoluchowski dynamics of the solvent (with k_B the Boltzmann constant and T the temperature). The longitudinal relaxation time τ_l is characteristic of the environment and the values for the most common organic solvents are well known and reported in literature.

When mixing quantum and classical dynamics, problems may arise with the dynamics not obeying the detailed balance rule. To address the issue, we neglect the off-diagonal matrix elements of $\hat{\rho}$ in the second and third line of eq. 7. With

this approximation, the master equation becomes:

$$\begin{aligned}\frac{\partial}{\partial t}\sigma_{ab}(F;t) = &- i\tilde{\omega}_{ab}(F)\sigma_{ab}(F;t) + \sum_{cd} R_{ab,cd}\sigma_{cd}(F;t) \\ &- \frac{\varepsilon_{or}}{\tau_l}\frac{\partial\sigma_{ab}(F;t)}{\partial F}(\rho_{aa}+\rho_{bb}) \\ &+ \frac{1}{\tau_l}\frac{\partial}{\partial F}\left(F\sigma_{ab}(F;t) + k_B T 2\varepsilon_{or}\frac{\partial}{\partial F}\sigma_{ab}(F;t)\right)\end{aligned} \tag{8}$$

Quite interestingly, this equation describes a Liouvillian dynamics where the frequency of the $b \to a$ transition is renormalized to account for solvatochromic effects: $\tilde{\omega}_{ab}(F) = \omega_{ab} - \frac{F}{\hbar}(\rho_{aa} - \rho_{bb})$.

Eq. 8 is exploited to describe the relaxation of an excited molecule in a polar environment upon impulsive excitation. At the equilibrium, we have a collection of molecules, each one experiencing a different reaction field, distributed according to the Boltzman law. To simulate the initial state, we diagonalize the F-dependent Hamiltonian for the solvated molecule in Eq. 2 on a grid of F values, to obtain the F-dependent eigenstates $|\psi_i(F)\rangle$. The equilibrium solvent distribution is calculated as $w(F, t = 0) = \exp(-E_1(F)/k_B T)$, where $E_1(F)$ is the lowest eigenstate (the only populated state at the equilibrium). Upon impulsive excitation, the solvent distribution is unaffected, but for each F, the molecule is driven in the coherent state

$$|\Psi^*(F)\rangle = \sum_{i=2}^{N} |\psi_i(F)\rangle\langle\psi_i(F)|\hat{\mu}|\psi_1(F)\rangle \tag{9}$$

Each $|\Psi^*(F)\rangle$ is then rotated on the basis of the eigenstates of the F-independent (i. e. gas phase) molecular Hamiltonian in eq. 1 and finally the initial state for the dynamics is obtained as $\hat{\sigma}(F,0) = w(F,0)|\Psi^*(F)\rangle\langle\Psi^*(F)|$.

The emission spectrum at time t' after the impulsive excitation is calculated defining the initial generating function as $\hat{\Omega}^f(F; t-t', t') = \hat{\mu}\hat{\sigma}(F;t')$, where $\hat{\sigma}(F;t')$ is the system reduced density matrix at time t' obtained integrating equation 8. Time evolution of $\hat{\Omega}^f(F; t-t', t')$ is evaluated according to equation 7 (using the whole $\hat{\rho}$ operator) and the dipole-dipole correlation function is obtained as $C^f_{\mu\mu}(t-t', t') = \langle\hat{\mu}(t-t')\hat{\mu}(t')\rangle = Tr_{\mathcal{S}}\left[\int dF \hat{\mu}'\hat{\Omega}^f(F; t-t', t')\right]$ where $\hat{\mu}'$ is the lower triangle of the dipole moment operator, that allows to extract only the emission contribution. The emission spectrum at t' is obtained

as the power spectrum of the Fourier transform of $C^f_{\mu\mu}(t-t',t')$ (damped with an exponential decay $e^{-t/a}$, $a = 30$ fs is used here).

The relaxation of the coherently excited state is evaluated integrating eq. 8 with the Short-Iterative-Arnoldi algorithm with a time-step of 1.5 fs and with a Krylov space of dimension 20. A full Redfield approach is adopted, meaning that all the terms of the four dimensional Redfield tensor $R_{ab,cd}$ are accounted for. We set the temperature to 298 K and $\gamma = 5$ ps^{-1}. Time resolved emission spectra are calculated integrating in the same conditions (i. e. temperature, dimension of the Krylov space etc...) eq 7 (with a time step of 0.15 fs.

We simulate the time evolution of emission spectra of NR in chloroform and DMF. We adopt the same model parameters (including the solvent relaxation energies) adopted to simulate steady-state spectra (see Fig. 2 and 3 main text). The only additional parameter entering the calculation of time-resolved spectra is the longitudinal relaxation time of the solvent, τ_l, and it is taken from literature data. Calculated time-resolved spectra of NR in chloroform and DMF are shown in the top panels of Fig. 9 (main text). The very good agreement with experiment validates the theoretical approach.

3 The model: dyes in solid matrices

3.1 Steady state spectra

To address the dye photophysics in solid matrices, we first estimate relevant relaxation energies from steady state-spectra. Absorption and Raman spectra are simulated adopting the same approach as for liquid solvents, in the hypothesis that the matrix is equilibrated to the ground state molecular polarity. Accordingly, we can estimate relevant matrix relaxation energies. Fig. 8 in main text and fig. S11 show results obtained for NR and DCM, respectively.

Emission spectra are more problematic. Indeed, it is not possible to reproduce experimental emission spectra neither considering a liquid environment, i.e.

assuming complete relaxation of the environment around the excited dye, nor considering the environment frozen at the ground state equilibrium. In the first hypothesis, we would get a too large red-shift of emission, while, in the second hypothesis, the emission spectrum would be largely blue shifted vs experiment. Following a recent and somewhat crude approximation, we consider two different contributions to polar solvation: a dynamical contribution with fast enough dynamics as to be equilibrated to the dye excited state before emission takes place, and a static contribution, that can be considered frozen at the ground state equilibrium in the timescale relevant to the emission process. A reaction field and a corresponding relaxation energy are assigned to the two components so that the Hamiltonian that describes the dye inside a matrix reads:

$$\hat{H} = \hat{H}_{mol} - F_{stat}\hat{\rho} + \frac{F_{stat}^2}{4\epsilon_{stat}} - F_{dyn}\hat{\rho} + \frac{F_{dyn}^2}{4\epsilon_{dyn}}. \tag{10}$$

Steady state emission spectra are finally calculated considering the Boltzmann distribution relevant to the ground state over F_{stat} and the one relevant to the excited state over F_{dyn}. Results for matrices are reported in the bottom panels of Fig. 8 (main text) and of fig. S11 for NR and DCM, respectively. The position of the absorption spectrum only depends on the total amount of coupling $\varepsilon_{or} = \varepsilon_{stat} + \varepsilon_{dyn}$, while the position of the emission spectrum depends also on the relative magnitude of the two relaxation energies.

3.2 Time-resolved spectra

Equations 7 and 8 can be extended to account for the interaction with the two fields F_{stat} and F_{dyn}. We then use our dynamical model to simulate time-resolved emission in mCBPCN and DPEPO. The dynamical component of the reaction field is associated with a time-dependent relaxation time $\tau_l = a + b(1 - e^{-ct})$, where a, b and c are adjustable parameters. Best results are obtained for $a = 100$ ps, $b = 14.9$ ns and $c = 0.0007$ ps^{-1} for DPEPO and $a = 20$ ps, $b = 5$ ns and $c = 0.001$ ps^{-1} for mCBPCN. Experimental data suggest for mCBPCN the presence of an initial very fast (<1 ps) relaxation, we therefore introduce in the first stage of the dynamics a very fast relaxation time: for the first 300 fs we consider a relaxation time of 500 fs, that is then switched off. In a first

approximation, this is equivalent to splitting the dynamical coordinate in two: F_{dyn1} with $\tau_l = 500$ fs and F_{dyn2} with $\tau_l(t)$.

Results in the bottom panels of Fig. 9 in main text are obtained. The first 1.5 ps of the main dynamics is calculated exactly as done for the solvents (initial coherent state, full Redfield, dimension of Krylov space 20 etc), and this allows to see the oscillations of the spectrum in the first hundreds of femtoseconds reflecting the fast coherent vibrational relaxation towards the Kasha state. Since with these dynamics we want to reach very long times (<ns) and the presence of two classical fields makes the calculation very demanding, the second part of the dynamics (from 1.5 ps on) is calculated evolving just the populations. The calculation significantly speeds up since we have to evolve just the N diagonal elements of the density matrix and not the whole N^2 matrix elements. Moreover, evolving just the populations allows to drastically reduce the dimension of the Krylov space required by the SIA algorithm to 3. This approximation is reliable since coherences definitely suppressed after 1.5 ps.